Article

Laser-Driven Very High Energy Electron/Photon Beam Radiation Therapy in Conjunction with a Robotic System

Kazuhisa Nakajima [1],*, Jianjun Yuan [2],†, Liming Chen [3],† and Zhengming Sheng [4,5],†

[1] Center for Relativistic Laser Science, Institute for Basic Science (IBS), Gwangju 500-712, Korea

[2] The Advanced Robotics Lab, School of Mechanical Engineering, Shanghai Jiao Tong University, Shanghai 200240, China; E-Mail: yuanjj@sjtu.edu.cn

[3] Beijing National Laboratory of Condensed Matter Physics, Institute of Physics, Chinese Academy of Sciences (CAS), Beijing 100080, China; E-Mail: lmchen@iphy.ac.cn

[4] Key Laboratory for Laser Plasmas (MoE) and Department of Physics and Astronomy, Shanghai Jiao Tong University, Shanghai 200240, China; E-Mail: zmsheng@sjtu.edu.cn

[5] Department of Physics, Scottish Universities Physics Alliance, University of Strathclyde, Glasgow G4 0NG, UK

† These authors contributed equally to this work.

* Author to whom correspondence should be addressed; E-Mail: naka115@dia-net.ne.jp; Tel.: +82-62-715-4753; Fax: +82-62-715-4705.

Academic Editor: Ken Ledingham

Abstract: We present a new external-beam radiation therapy system using very-high-energy (VHE) electron/photon beams generated by a centimeter-scale laser plasma accelerator built in a robotic system. Most types of external-beam radiation therapy are delivered using a machine called a medical linear accelerator driven by radio frequency (RF) power amplifiers, producing electron beams with an energy range of 6–20 MeV, in conjunction with modern radiation therapy technologies for effective shaping of three-dimensional dose distributions and spatially accurate dose delivery with imaging verification. However, the limited penetration depth and low quality of the transverse penumbra at such electron beams delivered from the present RF linear accelerators prevent the implementation of advanced modalities in current cancer treatments. These drawbacks can be overcome if the electron energy is increased to above 50 MeV. To overcome the disadvantages of the present RF-based medical accelerators, harnessing recent advancement of laser-driven plasma accelerators capable of producing 1-GeV electron beams in a 1-cm gas cell, we

propose a new embodiment of the external-beam radiation therapy robotic system delivering very high-energy electron/photon beams with an energy of 50–250 MeV; it is more compact, less expensive, and has a simpler operation and higher performance in comparison with the current radiation therapy system.

1. Introduction

Radiation therapy uses high energy radiation such as X-rays, gamma-rays, electrons, protons, heavy ions, and neutrons to kill cancer cells by damaging their DNA. Since radiation therapy can damage normal cells as well as cancer cells, treatment must be carefully planned to minimize such side effects. External-beam radiation therapy is most often delivered in the form of photon beams—either X-rays or gamma rays from a machine outside the body—in contrast to internal radiation therapy or brachytherapy, which use radioactive material placed in the body near cancer cells [1]. Since electron beams have a finite range after which the dose falls off rapidly in order to spare deeper normal tissue, electron beam therapy is typically used in the treatment of superficial tumors like cancer of skin regions or total skin, diseases of the limbs, and so on. For deeper regions, intra-operative electron radiation therapy might be applied. Many types of external-beam radiation therapy are delivered using a machine called a medical linear accelerator driven by RF power amplifiers such as magnetron and klystron, producing electron beams with an energy range of 6–20 MeV [2].

Technical advances in external-beam radiation therapy provide effective shaping of three-dimensional dose distributions and spatially accurate dose delivery by imaging verification. These technologies, including three-dimensional conformal radiation therapy (3D-CRT), intensity-modulated radiation therapy (IMRT), image guided radiation therapy (IGRT), stereotactic body radiation therapy (SBRT), and hadron therapy, increase the radiation dose to tumor areas and reduce radiation exposure to specific sensitive areas of surrounding normal tissue. In particular, the SBRT provides the radiation in a shorter time using smaller radiation fields and higher doses compared with the 3D-CRT by means of very sophisticated computer software and advanced treatment machines to deliver radiation very precisely to target areas in combination with a robotic manipulator and compact medical accelerator [1].

Medical robots are becoming revolutionary tools for a variety of clinical applications because of capabilities of exceeding human limitations on tremor reduction, repeatability, precision, and accuracy. In several areas of medicine, robots have been successfully developed and exploited: in 1985, a robot, the PUMA 560, was used to place a needle for a brain biopsy using CT guidance; in 1988, the PROBOT developed at Imperial College London was used to perform prostatic surgery by Senthil Nathan at Guy's and St. Thomas' Hospital, London [3]; tele-operated robots called da Vinci (Intuitive Surgical Inc., Sunnyvale, CA, USA) have been applied to cardiac and abdominal surgery, allowing soft tissue procedures to benefit from robotic enhancement [4]; and the Cyber Knife radiosurgery system (Accuray TM, Inc, Sunnyvale, CA, USA) was first used for treating various tumors by delivering non-isocentric radiation beam from a compact linac mounted on a robot [5–7]. The Cyber Knife was

said to be the first robotic device in which a human was permitted to be present within a robot workspace. Several generations of the Cyber Knife system have been successfully developed and applied since its initial inception in 1990.

However, the limited penetration depth and low quality of the transverse penumbra at the energy range of 6–20 MeV delivered from present medical RF linear accelerators currently prevent the aforementioned advanced modalities from being used in cancer treatment. These drawbacks can be overcome if the electron energy is increased above 50 MeV, whereby the penetration depth becomes longer and the transverse penumbra sharper, though the longitudinal penumbra is also increased. Since photon beams of maximal energies in the range of 150 MV to 250 MV have characteristics of depth dose deposition similar to reversed very high-energy (VHE) electron beams, VHE photon beams may be used separately or in combination with VHE electron beams to regulate the depth of dose maximum so that it can coincide with the depth of target volume [8].

Clinical effects of VHE electron beams on cancer therapy cannot be directly verified by measurement, since this beam type with 100 MeV-level energies is not available in small-scale facilities. Therefore, most of the investigations for verifying beam characteristics and dose distributions in specific cancer treatment have been studied by Monte Carlo simulations [8–12]. Referring to the results of Monte Carlo simulations carried out by DesRosiers *et al.* [8], depth-dose distributions from 200 MeV electron beams are illustrated for single-field, parallel opposed two-field, and orthogonal two-field arrangements as well as a 160 MeV proton beam with a Bragg peak at a depth of 15 cm, as shown in Figure 1. In the Monte Carlo simulation study [9] comparing intensity-modulated radiation therapy for prostate treatment with photon, proton, and VHE electron beams, the best conformity to the volume is achieved with proton beams, while target coverage for electron beams is comparable to or sometimes better than that provided by photon beams. Moreover, VHE electron beams provide a significant improvement over photon beams in the dose sparing of the sensitive structures and normal tissues. Monte Carlo simulations [10] of VHE electron beams with various energies have been performed to estimate dose distributions for a simulated lung tumor in comparison to state-of-the-art 6 MV photon beam therapy and a conventional 20 MeV electron beam therapy. This shows that electron energies of 75–100 MeV can produce superior quality compared to the photon beam and lower electron energies. It is also demonstrated that an 8 cc lung tumor could be treated with 100 MeV electrons to a 10 Gy in 1.3 s.

It is important for clinical application of VHE electron beams to consider dose contribution to the patient from neutrons and from induced radioactivity, and to evaluate neutron and radioactivity production from the standpoint of radiation protection. The mechanism of neutron production in the region of electron beam energies under consideration is determined by photodivision of nuclei via photo-nuclear reaction channels such as (γ,n), (γ,p), $(\gamma,2n)$, and (γ,pn) by Bremsstrahlung photons due to energy loss of VHE electrons and the small contribution of electrodivision by electrons. The analyses [8] on secondary particle production via the above-mentioned processes concluded that neutron and proton production in VHE electron beam therapy should not significantly affect equivalent doses in comparison with photon treatments, and that the required shielding should not be significantly greater than for 50 MeV electron and photon beams. Monte Carlo simulations [10] on contribution of secondary particles produced by Bremsstrahlung and electronuclear interactions to the dose from VHE

electron beams show that the estimated neutron dose is 1–2 orders of magnitude lower than that for scanning beam proton therapy and 15–18 MV photon IMRT.
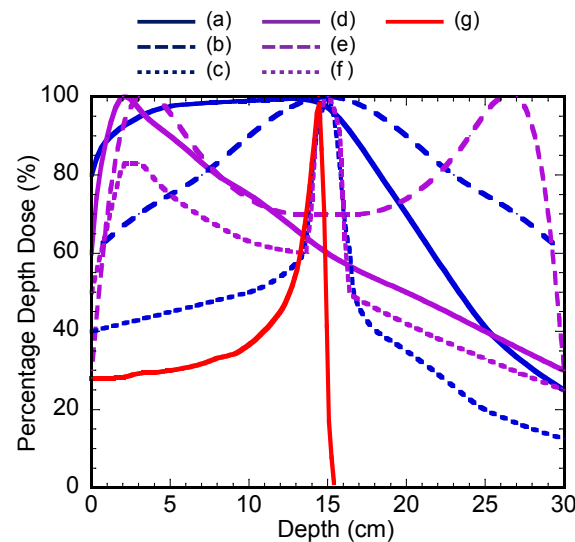

Figure 1. Percentage Depth Dose distributions from 200 MeV electron beams, referring to Monte Carlo simulation results carried out by DesRosiers *et al.* [8]: (**a**) single-field; (**b**) parallel opposed two-field; (**c**) orthogonal two-field, in comparison with those from a 15 MV photon beam for (**d**) single-field; (**e**) parallel opposed two-field; and (**f**) orthogonal two-field arrangements; and (**g**) 160 MeV single-field proton beam with Bragg peak, illustrated by Friesel *et al.* [13].

A proposed VHE electron beam therapy might utilize high-energy electron beams generated from a conventional RF-based linear accelerator comprising an electron injector, a main accelerating structure called LINAC [2], and a beam transport system, lastly followed by a gantry. The electron injector, typically composed of a photocathode RF gun or thermionic high-voltage DC gun and several buncher cavities for producing electron bunches. The LINAC is composed of a series of room-temperature or superconducting RF cavities with an accelerating gradient of the order of 10 MV/m. The beam transport system includes beam focusing and defocusing electro-quadrupole magnets. The gantry is mounted by vacuum beam transport systems and a series of beam steering and focusing electro-magnets. An overall size of a RF linac may require roughly a 50 m long facility for RF linac-based external-beam radiation therapy. Furthermore, a rotating gantry for multi-directional beam delivery may contribute a weight of the order of 100,000 kilograms. Therefore, the costs of construction and operation of such a facility may be prohibitively large so as to hinder the usage of conventional accelerator-based very high energy electron beam therapy systems in small-scale hospitals.

To date, active research has been carried out on the laser plasma acceleration concept [14] in order to achieve high-energy, high-quality electron beams with GeV energy in a cm-scale plasma [15–19], 1%-level energy spread [20], a 1-mm-mrad-level transverse emittance [21], and a 1-fs-level bunch duration [22], ensuring that the stability of reproduction is as high as that of the present high-power ultra-short-pulse lasers [23]. Recently, staged laser plasma acceleration [24,25] has been successfully demonstrated in conjunction with ionization-induced injection [26–28]. Relativistic electron beams

from ultraintense laser plasma interactions can be conceived of as compact particle accelerators, inspiring a wide range of applications of unique particle beam and radiation sources.

In this context, we present a new embodiment of the external-beam radiation therapy robotic system for delivering VHE electron/photon beams. This leads to a more compact and less expensive system with higher performance compared to previous techniques. Our proposed system comprises a drive laser, a plasma accelerator wherein the laser pulse generates VHE electron beams, a beam focusing system transporting electron beams from the plasma accelerator to a target in a patient, a photon beam target system generating VHE photon beams, a rotary gantry wherein the laser pulse is guided through a vacuum transport and focused onto the plasma accelerator, and a laser beam stabilizing system monitoring beam positions in the laser transport optics and correcting their alignment.

We organize the remainder of this article as follows. Section 2 presents a conceptual design for the laser-driven VHE electron/photon beam radiation therapy system. Section 3 presents a design example of laser in-frame robotic gantry. Section 4 describes discussions on feasibility, prospects for a new laser-driven radiation therapy system, and conclusions.

2. Laser-Driven Very-High-Energy Electron/Photon Beam Radiation Therapy System

The proposed radiation therapy system providing VHE electron/photon beams is composed of a drive laser system, laser plasma accelerator, electron beam focusing system, target system for the photon beam therapy, rotary gantry, and laser beam stabilizing system, as shown in Figure 2.
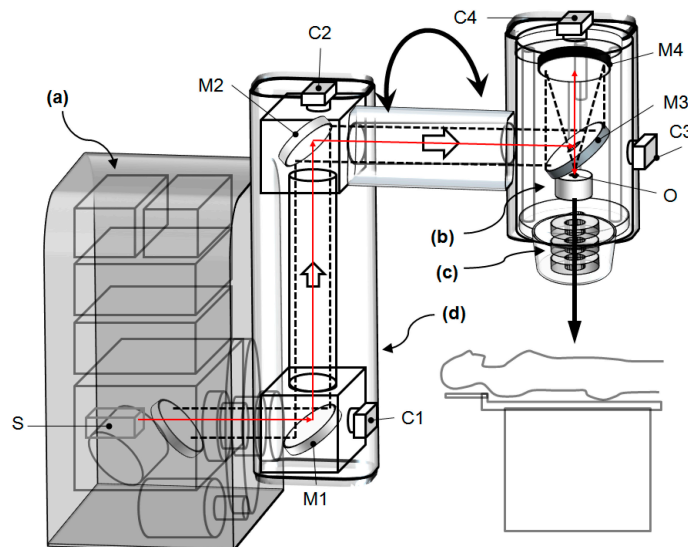

Figure 2. A conceptual sketch (not scaled) of the proposed radiation therapy system comprising (**a**) a drive laser system; (**b**) a laser plasma accelerator; (**c**) an electron beam focusing system; and (**d**) a laser-guiding vacuum transport embedded in a rotary gantry. Alignment of mirrors M1–M4 are corrected by a laser beam stabilizing system consisting of an alignment laser S and beam position monitor cameras C1–C4, to keep a laser pulse focus on the entrance of a laser plasma accelerator, O.

The drive laser system, comprising a front end and amplifier chain delivering energy-amplified pulses, is followed by an optical pulse compressor in order to form a drive laser pulse. The drive laser

pulse is guided through vacuum transport optics and focused onto the laser plasma accelerator, both of which are installed in the rotary gantry. In the laser plasma accelerator, drive laser pulses generate VHE electron beams. The beam focusing system transports the electron beams from the laser plasma accelerator to a target in a patient for VHE electron beam treatment, while the VHE electron beams are converted to photon beams in the target system for VHE photon beam treatment. The laser beam stabilizing system monitors beam positions in the laser transport optics and corrects their alignment. Major components of the laser-driven radiation therapy system are described in detail as follows.

2.1. Drive Laser System

The drive laser system for producing multi-TW laser pulses is based on the chirp pulse amplification technique [29], as shown in Figure 3. In this drive laser system, a low-energy laser pulse is produced by a front end, including a femtosecond oscillator and pulse stretcher wherein an oscillator pulse is stretched out in time, by means of a pair of diffraction gratings, having the effect of offsetting in time the various spectral components of the original low-energy pulse. The stretched pulse then has a lower peak power and a longer duration than the original pulse. An output pulse from the front end then seeds an amplifier chain. The pulse passing through this amplifier chain is amplified so as to generate a high-energy pulse. This amplified pulse is compressed timewise by an optical pulse compressor installed in a compressor vacuum chamber. The pulse compressor chamber is maintained at a pressure of the order of 10^{-4} Pa. The optical pulse compressor comprises a pair of diffraction gratings, grouping together in time the various spectral components of the pulse. The output pulse emerging from this optical compressor then has a very high energy and very short duration so that its energy and duration are optimized for producing an electron beam. A whole laser system, a vacuum pump, and the gantry drive system are installed in the cover case, as shown in Figure 2.
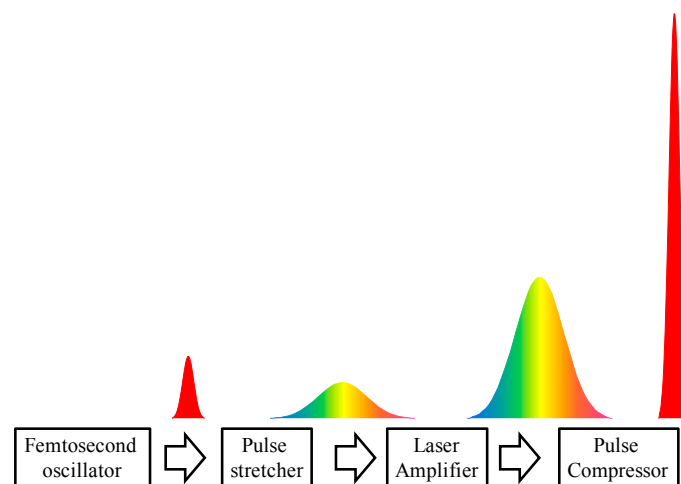

Figure 3. A schematic diagram of the drive laser system using the chirp pulse amplification technique.

For many practical applications of laser plasma accelerators, it is essential to employ high average power, high-efficiency drive lasers operated at the high repetition pulse rate. In particular, the stability and positioning precision of electron beams are critical issues for the medical accelerator performance [2]. For laser plasma accelerators, these issues are largely determined by the stability of the laser

performance, which is significantly improved as the pulse repetition rate increases. One such high average power laser system is the Coherent Amplifying Network (CAN) laser [30]. Here the conventional rod or slab laser amplifiers are replaced by a network of optical-fiber-based amplifiers. A femtosecond seed-laser pulse is repeatedly split and amplified through this network. The resulting pulses are then recombined coherently with precise individual phase control to produce a single amplified global laser pulse with a 1 J level of energy at the high repetition rate of 1 kHz to 1 MHz with efficiency of 30%–40%.

2.2. Design of Laser Plasma Accelerators for VHE Electron Beams

The laser plasma accelerator comprises an injector cell filled with a mixed gas, e.g., 98% helium gas mixed with 2% nitrogen, and an accelerator cell filled with a pure gas, e.g., hydrogen or helium gas. Figure 4 illustrates schematically a physical process for the wakefield excitation and electron trapping and acceleration in wakefields [26], which are generated when an intense laser pulse propagates a neutral mixed gas in the injector cell. The evolution of plasma electron density is shown in Figure 4a and the excited longitudinal wakefield is shown in Figure 4c. As shown in Figure 4b, helium and the outer shell electrons of nitrogen up to N^{5+} are fully ionized in the leading front of the laser pulse with an intensity of 1.5×10^{16} W/cm^2 to produce plasma electrons in the outer region of the laser pulse, of which the boundary is indicated by a thin dotted line. Since two inner shell (*K*-shell) electrons of N^{6+} and N^{7+} are ionized at a laser intensity higher than 1×10^{19} W/cm^2, the inner shell electrons are produced only near the peak intensity of the laser pulse, of which the intensity profile is indicated by a thick dotted line for the normalized vector potential $a_0 = 0.855 \times 10^{-9} I_L^{1/2}$(W/cm^2) λ_L(µm) $= 2$, where I_L is the intensity and λ_L is the laser wavelength. In Figure 4a, a solid curve indicates the evolution of the ionization level of nitrogen (the electron number of ionized nitrogen atom) along the propagation axis. A boundary of the plasma region containing the inner shell electrons from ionized N^{6+} and N^{7+} is indicated by a thin dashed line.

Plasma electrons contained in the boundary are blown out by radiation pressure (ponderomotive force) of the laser pulse with the relativistic intensity $a_0 \gg 1$ and form a narrow, dense electron sheath surrounding a spherical ion column behind the laser pulse, often referred to as a bubble, as shown in Figure 4b. Such charge separation generates a strong longitudinal electric field of the order of 100 GV/m at a plasma electron density of 10^{18} cm^{-3}, which is three orders of magnitude higher than an accelerating field of conventional RF accelerators. Inside the bubble, an electron undergoes a strong focusing force simultaneously. Hence, once electrons are trapped into a bubble, they are efficiently accelerated up to high energy of the order of 1 GeV over a dephasing length of the order of 1 cm, where accelerated electrons outrun a proper accelerating phase.

In the bubble (blowout) regime for $a_0 \geq 2$, since an electron-evacuated cavity shape is determined by balancing the Lorentz force of the ion sphere exerted on the electron sheath with the ponderomotive force of the laser pulse, the bubble radius R_B is approximately given as $k_p R_B = 2\sqrt{a_0}$, where $k_p = (4\pi r_e n_e)^{1/2}$ is the plasma wave number evaluated with the unperturbed on-axis density n_e, and the classical electron radius $r_e = e^2/m_e c^2 = 2.818 \times 10^{-13}$ cm with electron charge e, mass m_e, and vacuum light velocity c. The accelerating field E_z is given by $E_z/E_0 = (1/2)\alpha k_p R_B$, where $E_0 = mc\omega_p/e = 96$ (GV/m) $[n_e/10^{18}$(cm^{-3})$]^{1/2}$ is the non-relativistic wave-breaking field and α represents a factor taking into account the beam loading

and the difference between the simulation and theoretical estimation. The maximum energy gain W_{max}, limited due to dephasing, is given by $\Delta\gamma_{max} = W_{max}/m_e c^2 = (2/3)\alpha\kappa_{self}a_0(n_c n_e)$, where $n_c = m_e\omega_L^2/4\pi e^2 = \pi/(r_e\lambda_L^2)$ is the critical plasma density, $\kappa_{self} = (a_0^2/8)\{(1+a_0^2/2)^{1/2} - 1 - \ln([(1+a_0^2/2)^{1/2} + 1]/2)\}^{-1}$ is a correction factor of the group velocity for a self-guided relativistic laser pulse, of which the relativistic factor related to the group velocity $\beta_g = v_g/c$ is given by $\gamma_g^2 = 1/(1-\beta_g^2) = \kappa_{self}(\omega_L^2/\omega_p^2) = \kappa_{self}(n_c/n_e) = \kappa_{self}\gamma_{g0}^2$, where $\gamma_{g0} = \omega L/\omega_p$ is the relativistic factor for the linear group velocity for $a_0^2 \ll 1$. The dephasing length L_{dp} for the self-guided bubble regime is given by $k_p L_{dp} = (2/3)k_p R_B\gamma_g^2 = (4/3)\sqrt{a_0}\kappa_{self}(n_c/n_e)$. The important parameters of laser plasma accelerators (a list of symbols for designing parameters see in Table 1) for reaching a given energy E_b are summarized as follows [31]:

The operating electron plasma density is determined by

$$n_e = \frac{2}{3}\alpha\kappa_{self}a_0\frac{n_c}{\Delta\gamma_{max}} = 3\times10^{18}[\text{cm}^{-3}]\kappa_{self}a_0\left(\frac{0.8\mu m}{\lambda_L}\right)^2\left(\frac{200\text{MeV}}{E_b/\alpha}\right) \tag{1}$$

The accelerator length is set to be equal to the dephasing length as

$$L_{acc} = L_{dp} = \sqrt{\frac{3}{2}}\frac{(\Delta\gamma_{max}/\alpha)^{3/2}}{\pi\kappa_{self}^{1/2}a_0}\lambda_L = \frac{2.5[\text{mm}]}{\kappa_{self}^{1/2}a_0}\left(\frac{\lambda_L}{0.8\mu m}\right)\left(\frac{E_b/\alpha}{200\text{MeV}}\right)^{3/2} \tag{2}$$

The pump depletion length due to pulse front erosion becomes

$$L_{pd} = c\tau_L\frac{n_c}{n_e} = \frac{3}{2}\frac{c\tau_L\Delta\gamma_{max}/\alpha}{\kappa_{self}a_0} = \frac{5[\text{mm}]}{\kappa_{self}a_0}\left(\frac{\tau_L}{30\text{fs}}\right)\left(\frac{E_b/\alpha}{200\text{MeV}}\right) \tag{3}$$

The pulse duration required for satisfying a dephasing length longer than a pump depletion length is

$$\tau_L \geq 14[\text{fs}]\kappa_{self}^{1/2}\left(\frac{\lambda_L}{0.8\mu m}\right)\left(\frac{E_b/\alpha}{200\text{MeV}}\right)^{1/2} \tag{4}$$

The matched spot radius is given by

$$r_L = 3.1[\mu m]\frac{R_m}{\sqrt{\kappa_{self}a_0}}\left(\frac{\lambda_L}{0.8\mu m}\right)\left(\frac{E_b/\alpha}{200\text{MeV}}\right)^{1/2} \tag{5}$$

where

$$R_m = k_p r_L = \left\{\frac{\ln(1+a_0^2/2)}{\sqrt{1+a_0^2/2} - 1 - 2\ln[(\sqrt{1+a_0^2/2} + 1)/2]}\right\}^{1/2} \tag{6}$$

The corresponding matched power is

$$P_L = \frac{k_p^2 r_L^2 a_0^2}{32}P_c = 0.312[\text{TW}]\frac{a_0 R_m^2}{\kappa_{self}}\left(\frac{E_b/\alpha}{200\text{MeV}}\right) \tag{7}$$

where $P_c = 17\,n_c/n_e$ [GW] is the critical power for the relativistic self-focusing at the electron plasma density n_e. The required laser pulse energy is given by $U_L = P_L\tau_L$.

Assuming the beam loading efficiency $\eta_b = 1 - E_z^2/E_M^2$ defined by the fraction of the plasma wave energy absorbed by particles of the bunch with the root mean square (rms) radius σ_b, the beam-loaded field is given by $E_z = \sqrt{1-\eta_b}E_M = \alpha E_M$, where E_M is an accelerating field without beam loading. Thus a loaded charge is calculated as

$$Q_b \simeq \frac{e}{4k_L r_e} \frac{\eta_b k_p^2 \sigma_b^2}{(1-\eta_b)} \frac{E_z}{E_0} \left(\frac{n_c}{n_e}\right)^{1/2} = 76[\text{pC}] \frac{\eta_b k_p^2 \sigma_b^2}{(1-\eta_b)} \frac{E_z}{E_0} \left(\frac{n_e}{10^{18}\left[\text{cm}^{-3}\right]}\right)^{-1/2} \tag{8}$$

Using Equation (1) for plasma density n_e, the loaded charge is given by

$$Q_b = 44[\text{pC}] \frac{1-\alpha^2}{\alpha^{3/2}} \frac{k_p^2 \sigma_b^2}{\kappa_{\text{self}}^{1/2}} (\frac{\lambda_L}{0.8\,\mu m})(\frac{E_b}{200\text{MeV}})^{1/2} \tag{9}$$

A field reduction factor α for accelerating a charge of electrons Q_b up to the energy E_b is obtained from $\alpha^2 + C\alpha^{3/2} - 1 = 0$, where $C = (Q_b / 44\,\text{pC})\kappa_{\text{self}}^{1/2}(k_p^2 \sigma_b^2)^{-1}(\lambda_L / 1\,\mu m)^{-1}(E_b / 200\,\text{MeV})^{-1/2}$.
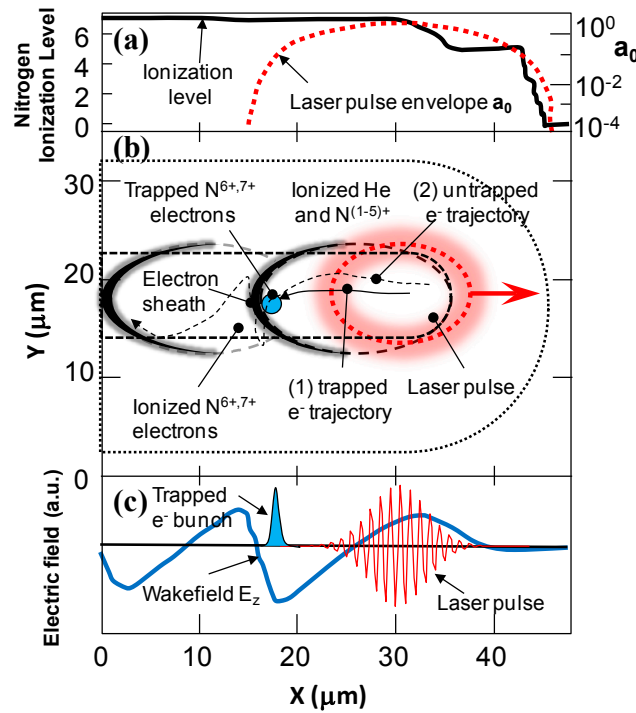

Figure 4. A physical process for tunnel ionization in shown in a He and N2 mixed gas, wakefield excitation, electron trapping due to ionization-induced injection mechanism, and acceleration in wakefields, schematically illustrated from particle-in-cell simulation results carried out by Pak *et al.* [26]. (**a**) The envelope of the normalized vector potential a_0 of the laser (dashed line) and the ionization state of nitrogen atoms (solid line) on axis; (**b**) Electron-density distribution from He and the *L*-shell electrons of nitrogen (inside dotted line) and from the *K*-shell electrons of nitrogen (inside dashed line), where electron (1) is ionized close to the axis and is trapped by the wakefield, while electron (2), ionized earlier and off-axis, slips and is not trapped; (**c**) The electric field of the laser pulse, the longitudinal electric field of the wake E_z, and the accelerated electron bunch.

The required electron beam charge is determined by the radiation therapy treatment plan, for example, a 10 cc lung tumor treatment with 100 MeV electrons to a dose of 10 Gy in 1 s. This treatment requires that a 1nC charge of 100 MeV electrons should be deposited over a 10 cc tumor volume in 1 s. At a repetition rate of 100 Hz, the laser plasma accelerator should provide an electron bunch with charge $Q_b = 10$ pC.

A laser-plasma driven VHE electron beam radiation therapy system is presented for the electron beam energies—50 MeV (Case A), 100 MeV (Case B), 150 MeV (Case C), 200 MeV (Case D), and 250 MeV (Case E). A drive laser pulse from the laser system is focused on the entrance of gas cells at the normalized laser field $a_0 = 2$ corresponding to the laser intensity $I = 5.5 \times 10^{18}$ W cm^{-2}. Self-guided propagation of such laser pulses in the gas cell requires the group velocity correction factor $\kappa_{self} = 1.19$ and the matched spot radius $R_m = 3.2$. The wakefield reduction factor α due to loaded charge Q_b is calculated from $\alpha^2 + C\alpha^{3/2} - 1 = 0$, assuming the electron beam radius $k_b\sigma_b = 1$, where the coefficients are $C = 0.50, 0.35, 0.29, 0.25,$ and 0.22 as $\alpha = 0.80, 0.85, 0.88, 0.89,$ and 0.90, respectively, for Case A to E. The main parameters for the laser plasma accelerator are provided as shown in Table 2.

Table 1. A list of symbols for designing laser plasma accelerators.

Parameters	Symbols
Speed of light in vacuum	c
Laser wavelength	λ_L
Laser angular frequency	ω_L
Laser intensity	I_L
Laser spot radius	r_L
Laser pulse duration	τ_L
Laser peak power	P_L
Laser pulse energy	U_L
Normalized vector potential	a_0
Normalized matched spot radius	R_m
Critical power for relativistic self-focusing	P_c
Electron charge	e
Electron mass	m_e
Classical electron radius	r_e
Plasma electron density	n_e
Plasma electron frequency	ω_p
Plasma wave number	k_p
Critical plasma density	n_c
Group velocity	v_g
Normalized group velocity	β_g
Relativistic factor related to the group velocity	γ_g, γ_{g0}
Correction factor of the group velocity	κ_{self}
Bubble radius	R_B
Accelerating electric field with beam loading	E_Z
Accelerating electric field without beam loading	E_M
Non- relativistic wave-breaking field	E_0
Reduction factor of the accelerating field	α
Maximum energy gain	W_{max}
Design electron beam energy	E_b
Normalized maximum energy gain	$\Delta\gamma_{max}$
Dephasing length	L_{dp}
Accelerator length	L_{acc}
Pump depletion length	L_{pd}
Electron beam charge	Q_b
Root mean square electron beam radius	σ_b
Beam loading efficiency	η_b

For Case E, the laser system should be capable of delivering a 150 mJ drive pulse with 20 fs duration at 100 Hz to the laser plasma accelerator for producing a 10 pC electron bunch. The electron beam energy can be controlled by adjusting the laser pulse energy, plasma density, and accelerator length.

Table 2. Main parameters of laser plasma accelerators for VHE electron beam radiation therapy system.

Case	A	B	C	D	E
Electron beam energy [MeV]	50	100	150	200	250
Laser wavelength [μm]	0.8	0.8	0.8	0.8	0.8
Laser energy per pulse [mJ]	33	63	92	121	149
Peak power [TW]	1.7	3.2	4.6	6.0	7.5
Pulse duration [fs]	20	20	20	20	20
Matched spot radius [μm]	3.6	5.0	6.0	6.9	7.6
Plasma density [10^{19} cm^{-3}]	2.3	1.2	0.8	0.6	0.5
Accelerator length [mm]	0.2	0.5	0.9	1.4	1.9
Charge per bunch [pC]	10	10	10	10	10

2.3. Simulations on Laser Plasma Accelerators

Electron beams can be produced and accelerated in the injector cell driven by the same laser pulse as that in the accelerator cell, relying on the self-injection mechanism [32,33]. We studied the production of high-quality electron beams with energy of 300 MeV and a charge of ~100 pC by means of the particle-in-cell (PIC) simulations. The self-injection electron beam production has been investigated by the 2D PIC simulation code (VORPAL) [34], using the 2D moving window, of which the cell size was 94×90 μm^2 and the number of simulation cells 1792×256, respectively, assuming He^{2+} immobile ions and four electrons per simulation cell. Figure 5a,b shows the simulation result of the electron density distribution and the electron energy spectrum, respectively, at the propagation distance $z = 3$ mm for the drive laser pulse with wavelength $\lambda_L = 0.8$ μm, the initial normalized field $a_0 = 4$, spot radius $r_L = 15$ μm, and pulse duration $\tau_L = 27$ fs, which is focused into uniform plasma with electron density $n_e = 2 \times 10^{18}$ cm^{-3}. In this example, the focused spot size was chosen from the condition $k_p R_B = k_p r_L = 2\sqrt{a_0}$ to form a spherical bubble wake with radius R_B. For this condition, the accelerated electron beam has energy of 320 MeV, relative rms energy spread of 4%, and charge of 100 pC. As shown in Figure 5c,d, increasing the focused spot radius up to $r_L = 30$ μm, the electron beam energy decreases down to 210 MeV, while the energy spread becomes significantly worse as the trapped beam charge increases. This may be attributed to longitudinal expansion of the bubble size [33] and beam loading effects.
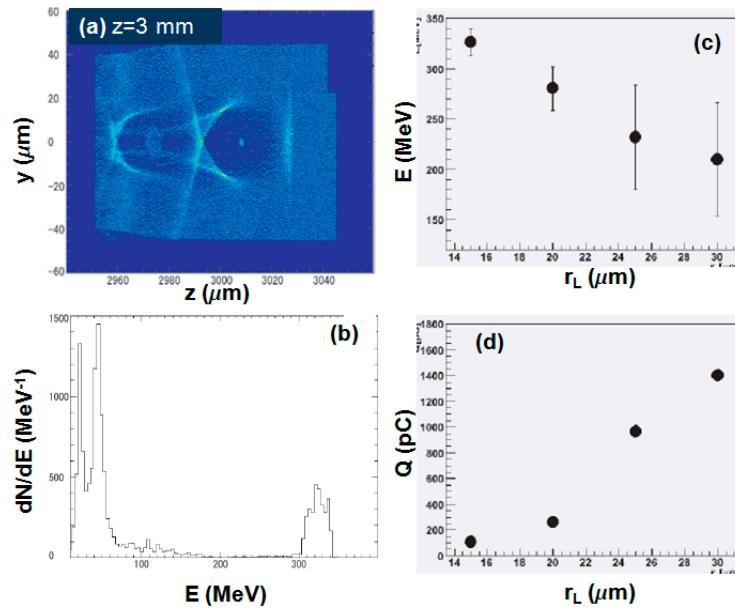
Figure 5. 2D PIC simulation results of laser wakefield acceleration driven by a laser pulse with wavelength λ_L = 0.8 μm, normalized field a_0 = 4, spot radius r_L = 15 μm, and pulse duration τ_L = 27 fs at plasma density n_e = 2 × 10^{18} cm^{-3}; (**a**) Electron-density distribution at the propagation distance z = 3 mm; (**b**) Electron energy spectrum at z = 3 mm; (**c**) Energy and energy spread; and (**d**) trapped electron charge as a function of spot radius.

2.4. An Embodiment of Laser-Driven VHE Electron- and Photon-Beam Sources

Figure 6 schematically illustrates the gantry head, the most crucial part of the radiation therapy system, where are installed a final focus optics, electron laser plasma accelerator, and beam focusing system for VHE electron beam therapy or Bremsstrahlung conversion target for VHE photon beam therapy. The ultrashort intense laser pulse is focused by a spherical mirror or off-axis parabolic mirror on the entrance of a two-stage gas cell, of which the first cell referred to an injector is filled with a mixed gas, e.g., helium gas mixed with nitrogen, and the second cell referred to as an accelerator is filled with a pure gas, e.g., hydrogen or helium. The gases are fed through a gas flow control system to the two-stage gas cell separately at the different pressures. According to the abovementioned mechanism, in the injector of the gas cell, the laser pulse excites large-amplitude plasma wakefields, of which an accelerating electric field can trap plasma electrons exclusively out of the inner shell electrons and accelerate them owing to ionization-induced injection. A pre-accelerated electron beam from the injector is further accelerated to the relativistic energy in the accelerator gas cell, where the laser pulse generates plasma wakefields.

A collimated electron beam from the laser plasma accelerator is provided to the target in the patient by the beam focusing system comprising permanent quadrupole magnets, as shown in Figure 6. The field gradient of the two dimensional Halbach-type permanent quadrupole magnet (PMQ) is given by $B' = 2B_r(r_i^{-1} - r_o^{-1})$, where B_r is the tip field strength, r_i is the inner radius, and r_0 is the outer radius of PMQ [35]. With B_r = 1.45 T for Nd-Fe-B type rare earth magnet (Nd$_2$Fe$_{14}$B) with PM Grades N50 and r_i = 2.5 mm, one can obtain the field gradient $B' = 1160$ [T/m]$(1 - 2.5$[mm]$/r_o)$. The beam focusing system comprises two or three permanent quadrupole magnets (PMQs), e.g., a doublet (FD) or a triplet

(FDF) installed into a housing chamber. For the photon beam therapy, VHE photons can be produced from a photon beam target system comprising a Bremsstrahlung conversion target and collimator, where the beam focusing system is retracted and electron beams are directly irradiated, as shown in Figure 6.
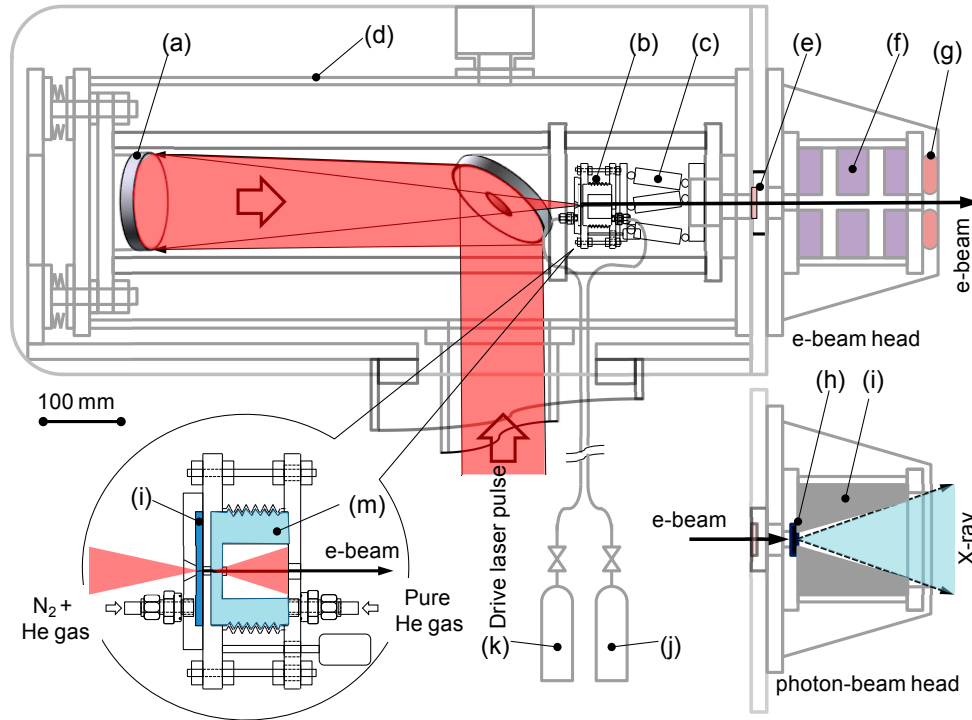

Figure 6. A schematic of the gantry head, comprising (**a**) a final focus mirror; (**b**) two-stage gas cell; (**c**) multi-axis positioning stage for the gas cell, e.g., miniature 6-axes hexapod; (**d**) vacuum chamber containing the laser plasma accelerator and drive laser optics; (**e**) vacuum window thin film, e.g., beryllium, for separating vacuum and air; (**f**) beam focusing system assembled three permanent quadrupole magnets; (**g**) current transformer for measuring electron beam charge; (**h**) Bremsstrahlung conversion target; (**i**) photon beam collimator; (**j**) pure He gas fed to the accelerator; (**k**) N_2 and He mixed gas fed to the injector; (**l**) injector gas cell; and (**m**) accelerator gas cell.

2.5. Laser Beam Stabilizing System

The misalignment in the laser transport optics due to movement of the rotary gantry can be retrieved by means of a laser beam stabilizing system, as shown in Figure 2. The drive laser pulse delivered from a fixed mirror inside the pulse compressor chamber is guided by a mirror system comprising M1, M2, M3, and M4 to the entrance O of the laser plasma accelerator. A position of an alignment beam provided by a laser S is monitored at a charge coupled device (CCD) camera, C1 to C4, viewing each mirror, M1 to M4. Generally, once movement of the gantry causes displacement $\Delta C_{ix,y}$ of the position of the alignment laser beam on the *i*th mirror for *x*- and *y*-direction, respectively, a correction angle of the *i*th mirror is given by $\Delta \theta_{ix,y} = \Delta C_{i-1x,y} / s_{i-1} - \Delta C_{i+1x,y} / s_i$, where s_i is a distance between the *i*th mirror and the *i*+1th mirror in order to keep the final focus position O fixed. These angular corrections of each mirror are set by means of two precision actuators, e.g., piezoelectric actuators, integrated into a

mirror holder, installed in a vacuum box. A process measuring the laser beam position on each mirror and then correcting angles of the mirror may be repeated until the laser beam positions are stabilized.

3. Conceptual Design of Laser In-Frame Robotic Gantry

The program of developing a new laser in-frame robot for very high-energy electron/photon beam therapy is to provide revolutionary equipment that overcomes some of the problems existing in the radiation therapy system, such as Cyber Knife [5], for instance, which is a combination of a small-sized X-ray linac and a traditional industrial manipulator in its structure. Intense laser pulses are generated and transmitted to the base of the manipulator, then through its frame and joints, and are finally delivered to the accelerator equipped at the tip of the manipulator, where the electron beam is generated. A laser beam with a diameter of the order of 50 mm has to be transmitted in vacuum before it is delivered to the accelerator. Therefore the design feature of the robot arm should meet all the requirements on payload, positioning accuracy, and an inside vacuum hollow structure with minimum 80 mm-level diameter, as well as keeping the manufacturing costs as low as possible. In our proposal, all the frames and joints are designed in a large-sized internal vacuum hollow structure and then all of the driven components have to be outward distributed.

It is clear that five is the minimum necessary number of DOFs (degrees of freedom) for the treatment by electron/photon beam to cancer cells, by adjusting the position and pose of the beam. The robot may be capable of providing five or fewer DOFs, and other equipment, such as the treatment couch, may contribute the rest (one or more DOFs). For medical use, the robotic arm is also required to be small, compact, hygienic, and noiseless. The five DOFs are waist rotation, elbow pitch, and shoulder pitch, as well as the tilts of the wrist with two further revolute joints. Among them, the rotary joint (especially for waist rotation), which acts as an essential driving/guiding component and supporting structure, is of extreme importance. At the beginning of the treatment, the joints will find their relative location of the lesion programmed by the computer. During the treatment, the irradiated point should be adjusted immediately once the data of the location of the lesion changes. This system must be real-time and accurate-positioning. This rotary joint needs to have a vacuum channel inside, the diameter of which should be at least 80 mm to serve for the laser transmission. There is no such commercial mechanism that meets these requirements among the present industrial manipulators. Therefore, the design is an extremely difficult and challenging task compared to a traditional manipulator. Here we propose a low cost but high positioning accuracy rotary joint, thereby reducing the cost of the package of this medical robotic system. The rotary joint is able to withstand the weight of the whole robotic arm device itself as well as the external load. Fast and accurate positioning to the pathological location determined by the medical plan is promised. In the course of treatment, the end of the robot arm is therefore able to keep changing subtly at any time according to the positioning data, and to adjust the irradiation site to achieve accuracy of real-time treatment.

The main task of our research is developing a new laser in-frame robot with five degrees of freedom to guide the laser beam inside. For medical use, the robotic arm is required to be small and compact to ensure the laser beam positioning accuracy at the manipulator end as well as the lowest possible cost. In addition, the robotic arm shall maintain an internal hollow for implantation of a vacuum optical path. The design of the robotic rotary joint is one of the most crucial steps to realize these objectives.

Therefore, the design features of the rotary joint should be able to meet the requirements of the work load of the robot arm and the accelerator, the rotational positioning accuracy of the rotary mechanism, as well as reducing the manufacturing cost of the entire robotic system. Compared to traditional manipulator design, this is a difficult and challenging task.

This rotary joint is mainly used in the follow-up medical manipulator, and therefore multiple rotation speeds should be able to be provided. According to the treatment plan, the accelerator at the end of the robotic arm is positioning at any location within a sphere that keeps a certain distance from the lesion area. Here is the hypothesis for rotational speed of the rotary joint: Firstly, during the initialization of a surgery, the manipulator needs to have a faster positioning speed to ensure that the electron accelerators at the end of the robotic arm quickly move to the patient's lesions nearby and are ready for subsequent treatment. Secondly, a relatively lower working speed, under the control of the computer program, is serving as the precise positioning of patients' lesions during the radiosurgery process.

Figure 7 shows a detailed design of the rotary joint and a whole aspect of the manipulator. A servo motor is used to drive a ball screw for rotation, then a slider together with the screw nut for translation. Several steel cables or steel flat belts are wound around the rotary waist and fixed to the slider for motion transmission. This connection allows the motor to finally drive the rotary joint to do stable rotation in both clockwise and anticlockwise directions. A tension-adjusting mechanism ensures the transmission stiffness of the steel cables or belts is at a high level, and at the same time enables precise motion with no backlash. The rotary joint is finally covered by an outside box for a clean aspect, as shown in Figure 7.
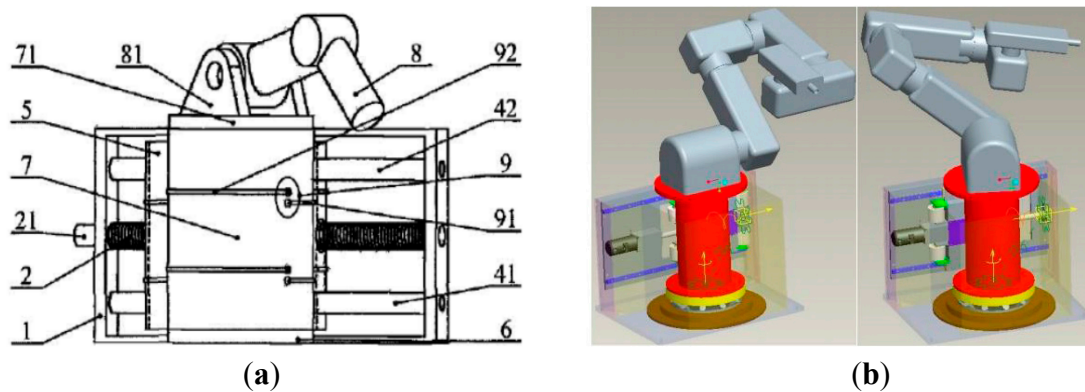

(a) **(b)**

Figure 7. A novel design of laser-in-frame robotic manipulator for laser-driven VHE electron/photon beam therapy. (**a**) The design concept of rotary joint; (**b**) The whole manipulator.

With the analysis of the actual operation conditions of the VHE electron beam radiation therapy system, the whole upper robot arm is simplified to be one simple beam with a length of 1.5 m and mass of 40 kg. The laser electron accelerator is then represented by a mass point of 80 kg. Right below the arm is the cylindrical rotational waist, which has a height of about 0.3 m and a diameter of 200 mm. With this simplified model, it becomes easy and convenient to calculate the approximate working force loaded on the rotary joint and the velocity of both working condition and positioning condition. As a result of preliminary calculations, the suitable reduction ratio of this rotary joint is about 125. At

working conditions, the velocity of the power screw is about 50 mm/s, while at the positioning condition it is about 10 times higher.

4. Discussion and Conclusions

We present a conceptual design for a laser plasma accelerator-driven very high energy electron/photon beam radiation therapy robotic system comprising a drive laser system, laser plasma accelerator, electron beam focusing system, photon beam target system, main-body of robot, and laser beam stabilizing system. The drive laser system produces energy-amplified high-energy laser pulses. The intense laser pulses are guided through the inside vacuum structure of the main body of a robot into the accelerator chamber attached at the head of the main body of the robot, and focused onto the laser plasma accelerator mounted in the accelerator chamber, where they finally generate electron beams. The electron beam focusing system transports electron beams to the target in a patient, and the photon beam target system also generates photon beams for VHE electron/photon beam radiation therapy. The main body of the robot delivers the electron/photon beam to the target in a patient from multiple directions. The laser beam stabilizing system monitors laser beam positions and corrects their alignment during treatment.

From a clinical point of view, since protons and heavy ions have a finite range in the radiation dose distribution along the beam path, where the dose increases slowly with the depth and then rises very steeply to produce a Bragg peak, as shown in Figure 1, generally speaking, the proton and carbon ion beams therapies are superior even to the highest technology X-ray therapy. However, in reality most radiation therapy (~99%) is currently carried out with X-ray beams of 6–20 MV photons because of the cost-effectiveness and the high capital cost of constructing and maintaining infrastructures to produce such proton and carbon ion beams, including large-scale particle accelerators such as cyclotrons, synchrotrons, beamlines, gantries, and radiation shielding in a clinical environment as well as the human resources for operating such a large facility. To date, Japan has the world's largest number of hadron therapy facilities (nine proton and four heavy ion therapy facilities) [36]. It is said that a new hadron facility 3000 square meters in area requires roughly $100 million for initial construction and several million dollars for annual maintenance [37], compared to $10 million for the highest technology X-ray therapy system in a clinic 100 square meters in area. In addition, the cost of treatment requires about $30,000 for proton therapy [37], compared to $6000 for X-ray therapy. Considering the current prices for a commercial multi-TW laser and robotic system, one may envisage a similar cost for the installation, operation, and treatment of the proposed laser-based VHE electron/photon beam therapy system as that of the X-ray therapy system.

In this context, if electron beams with 50–250 MeV energies, which are not currently available in small-scale facilities, could be generated with a compact medical accelerator having a similar or even smaller size, such VHE electron beams would provide us with clinical effects superior to the present X-ray therapy, even comparable to proton beam therapy in terms of cost-effectiveness, compactness, and simplicity, which are important requirements for ubiquitous high-technology radiation therapy.

Here we propose a new radiation therapy device that makes it possible to deliver 50–250 MeV VHE electron beams from a compact laser-driven plasma-based accelerator, which can be mounted on a gantry with laser optics installed in a robotic arm and controlled for delivering narrow collimated

beams—so-called pencil beams—to tumors in a patient from multiple directions for intensity-modulated radiation therapy (IMRT) using pencil beam scanning (PBS), in conjunction with image guided radiation therapy (IGRT). Technologies of the laser in-frame robot developed for VHE electron beams will pave the way for laser-driven proton beam therapy as well, which uses protons with the kinetic energy range in the medical window 70–300 MeV, though much higher intensity lasers will be needed for the production of such high-energy protons due to laser–plasma interactions.

Although the achievement of current laser plasma electron acceleration experiments basically carried out in a single-shot mode may not ensure the performance of laser-driven electron beams in practical applications, the requirements for VHE electron beams with energies of 50–250 MeV, an rms energy spread of the order of 5%, and an electron charge of the order of 10 pC have been demonstrated by previous experiments on a two-staged laser wakefield accelerator comprising an injector and accelerator cells in conjunction with ionization-induced injection [24,25]. The most crucial requirement for VHE electron/photon beam radiation therapy may be a shot-to-shot energy stability of the order of 1% and pointing stability of the order of 1 mrad for IMRT with PBS. Since these stabilities are dominantly attributed to the stability of drive lasers, the current limits of a few percent-level stability at the repetition rate of the order of 1 Hz operation would be improved to the level of less than 1% by increasing the repetition rate of drive laser pulses to 100 Hz. Furthermore, the use of coherent combining fiber lasers capable of producing VHE electron beams could replace the rotary vacuum channels with flexible fibers for transporting laser pulses to the gas cell, removing the need for a large part of the guiding optics and aligning system as well as increasing the repetition rate and efficiency of the drive laser.

In conclusion, the very high energy electron/photon beam radiation therapy robotic system proposed is more compact and efficient, less expensive, and offers simpler and safer operation in addition to higher performance compared to previous techniques. This will lead to cost-effective, ubiquitous high-technology radiation therapy including photon, electron, and proton beams, in conjunction with advanced robot technologies.

Acknowledgments

Author Contributions

Kazuhisa Nakajima contributed to the design and analysis of laser plasma accelerators and their manuscript preparation. Jianjun Yuan contributed to the design and analysis of the robotic gantry and the manuscript preparation. Liming Chen and Zhengming Sheng contributed to discussions.

Conflicts of Interest

The authors declare no conflict of interest.

References

1. National Cancer Institute at the National Institutes of Health, Radiation Therapy for Cancer. Available online: http://www.cancer.gov/cancertopics/factsheet/Therapy/radiation (accessed on 25 September 2013).
2. Whittum, D.H. Microwave Electron Linacs for Oncology. In *Reviews of Accelerator Science and Technology*; Chao, A.W., Chou, W., Eds.; World Scientific: Singapore, 2009; Volume 2, pp. 63–92.
3. Kwoh, Y.S.; Hou, J.; Jonckheere, E.A.; Hayall, S. A robot with improved absolute positioning accuracy for CT guided stereotactic brain surgery. *IEEE Trans. Biomed. Eng.* **1988**, *35*, 153–161.
4. Coste-Manière, È.; Olender, D.; Kilby, W.; Schulz, R.A. Robotic whole body stereotactic radiosurgery: Clinical advantages of the CyberKnife integrated system. *Int. J. Med. Robot. Compt. Assist. Surg.* **2005**, *1*, 28–39.
5. Adler, J.R., Jr.; Chang, S.D.; Murphy, M.J.; Doty, J.; Geis, P.; Hancock, S.L. The Cyberknife: A frameless robotic system for radiosurgery. *Stereotact. Funct. Neurosurg.* **1997**, *69*, 124–198.
6. Dieterich, S.; Gibbs, I.C. The Cyber Knife in Clinical Use: Current Roles, Future Expectations. In *IMRT, IGRT, SBRT*; Meyer, J.L., Ed.; Karger: Basel, Switzerland, 2011; Volume 43, pp. 181–194.
7. Murray, L.J.; Robinson, M.H. Radiotherapy: Technical aspects. *Medicine* **2010**, *39*, 698–704.
8. DesRosiers, C.; Moskvin, V.; Bielajew, A.F.; Papiez, L. 150–250 MeV electron beams in radiation therapy. *Phy. Med. Biol.* **2000**, *45*, 1781–1805.
9. Yeboah, C.; Sandison, G.A. Optimized treatment planning for prostate cancer comparing IMPT, VHEET and 15 MV IMXT. *Phys. Med. Biol.* **2002**, *47*, 2247–2261.
10. Loo, B.W.; Maxim, P.G.; Dolgashev, V.A. Pluridirectional very high electron energy radiation therapy systems and processes. U.S. Patent 13/765,017, 12 February 2013.
11. Subiel, A.; Moskvin, V.; Welsh, G.H.; Cipiccia, S.; Reboredo, G.D.; Evans, P.; Partridge, M.; DesRosiers, C.; Anania, M.P.; Cianchi, A.; *et al*. Dosimetry of Very High Energy Electrons (VHEE) for radiotherapy applications. *Phys. Med. Biol.* **2014**, *59*, doi:10.1088/0031-9155/59/19/5811.
12. Moskvin, V.; Subiel, A.; Desrosiers, C.; Wiggins, M.; Maryanski, M.; Mendonca, M.; Boyd, M.; Sorensen, A.; Cipiccia, S.; Issac, R.; *et al*. Characterization of the Very High Energy Electrons, 150–250 MeV (VHEE) Beam Generated by ALPHA-X Laser Wakefield Accelerator Beam Line for Utilization in Monte Carlo Simulation for Biomedical Experiment Planning. *Med. Phys*. **2012**, *39*, doi:10.1118/1.4735561.
13. Friesel, D.L.; Antaya, T.A. Medical Cyclotrons. In *Reviews of Accelerator Science and Technology*; Chao, A.W., Chou, W., Eds.; World Scientific: Singapore, 2009; Volume 2.
14. Tajima, T.; Dawson, J.M. Laser electron accelerator. *Phys. Rev. Lett.* **1979**, *43*, 267–270.
15. Leemans, W.P.; Nagler, B.; Gonsalves, A.J.; Toth, C.; Nakamura, K.; Geddes, C.G.R.; Esarey, E.; Schroeder, C.B.; Hooker, S.M. GeV electron beams from a centimetre-scale accelerator. *Nat. Phys.* **2006**, *2*, 696–699.
16. Clayton, C.E.; Ralph, J.E.; Albert, F.; Fonseca, R.A.; Glenzer, S.H.; Joshi, C.; Lu, W.; Marsh, K.A.; Martins, S.F.; Mori, W.B.; *et al*. Self-guided laser wakefield acceleration beyond 1 Gev using ionization-induced injection. *Phys. Rev. Lett.* **2010**, *105*, doi:10.1103/PHYSREVLETT.105.105003.

17. Lu, H.; Liu, M.; Wang, W.; Wang, C.; Liu, J.; Deng, A.; Xu, J.; Xia, C.; Li, W.; Zhang, H.; *et al.* Laser wakefield acceleration of electron beams beyond 1 GeV from an ablative capillary discharge waveguide. *Appl. Phys. Lett.* **2011**, *99*, doi:10.1063/1.3626042.

18. Wang, X.; Zgadzaj, R.; Fazel, N.; Li, Z.; Yi, S.A.; Zhang, X.; Henderson, W.; Chang, Y.Y.; Korzekwa, R.; Tsai, H.E.; *et al.* Quasi-monoenergetic laser-plasma acceleration of electrons to 2 GeV. *Nat. Commun.* **2013**, *4*, doi:10.1038/ncomms2988.

19. Kim, H.T.; Pae, K.H.; Cha, H.J.; Kim, I.J.; Yu, T.J.; Sung, J.H.; Lee, S.K.; Jeong, T.M.; Lee, J. Enhancement of electron energy to the multi-GeV regime by a dual-stage laser-wakefield accelerator pumped by petawatt laser pulses. *Phys. Rev. Lett.* **2013**, *111*, doi:10.1103/PhysRevLett.111.165002.

20. Kameshima, T.; Hong, W.; Sugiyama, K.; Wen, X.; Wu, Y.; Tang, C.; Zhu, Q.; Gu, Y.; Zhang, B.; Peng, H.; *et al.* 0.56 GeV laser electron acceleration in ablative-capillary-discharge plasma channel. *Appl. Phys. Exp.* **2008**, *1*, doi:10.1143/APEX.1.066001.

21. Karsch, S.; Osterhoff, J.; Popp, A.; Rowlands-Rees, T.P.; Major, Z.; Fuchs, M.; Marx, B.; Hörlein, R.; Schmid, K.; Veisz, L.; *et al.* GeV-scale electron acceleration in a gas-filled capillary discharge waveguide. *New J. Phys.* **2007**, *9*, 415–425.

22. Lundh, O.; Lim, J.; Rechatin, C.; Ammoura, L.; Ben-Ismail, A.; Davoine, X.; Gallot, G.; Goddet, J.P.; Lefebvre, E.; Malka, V.; *et al.* Few femtosecond, few kiloampere electron bunch produced by a laser-plasma accelerator. *Nat. Phys.* **2011**, *7*, 219–222.

23. Hafz, N.A.M.; Jeong, T.M.; Choi, I.W.; Lee, S.K.; Pae, K.H.; Kulagin, V.V.; Sung, J.H.; Yu, T.J.; Hong, K.H.; Hosokai, T.; *et al.* Stable generation of GeV-class electron beams from self-guided laser-plasma channels. *Nat. Photon.* **2008**, *2*, 571–577.

24. Liu, J.S.; Xia, C.Q.; Wang, W.T.; Lu, H.Y.; Wang, C.; Deng, A.H.; Li, W.T.; Zhang, H.; Liang, X.Y.; Leng, Y.X.; *et al.* All-optical cascaded laser wakefield accelerator using ionization-induced injection. *Phys. Rev. Lett.* **2011**, *107*, doi:10.1103/PhysRevLett.107.035001.

25. Pollock, B.B.; Clayton, C.E.; Ralph, J.E.; Albert, F.; Davidson, A.; Divol, L.; Filip, C.; Glenzer, S.H.; Herpoldt, K.; Lu, W.; *et al.* Demonstration of a narrow energy spread, similar to ~0.5 GeV electron beam from a two-stage laser wakefield accelerator. *Phys. Rev. Lett.* **2011**, *107*, doi:10.1103/PhysRevLett.107.045001.

26. Pak, A.; Marsh, K.A.; Martins, S.F.; Lu, W.; Mori, W.B.; Joshi, C. Injection and trapping of tunnel-ionized electrons into laser-produced wakes. *Phys. Rev. Lett.* **2010**, *104*, doi:10.1103/PhysRevLett.104.025003.

27. McGuffey, C.; Thomas, A.G.R.; Schumaker, W.; Matsuoka, T.; Chvykov, V.; Dollar, F.J.; Kalintchenko, G.; Yanovsky, V.; Maksimchuk, A.; Krushelnick, K.; *et al.* Ionization induced trapping in a laser wakefield accelerator. *Phys. Rev. Lett.* **2010**, *104*, doi:10.1103/PhysRevLett.104.025004.

28. Xia, C.; Liu, J.; Wang, W.; Lu, H.; Cheng, W.; Deng, A.; Li, W.; Zhang, H.; Liang, X.; Leng, Y.; *et al.* Effects of self-focusing on tunnel-ionization-induced injection in a laser wakefield accelerator. *Phys. Plasmas* **2011**, *18*, doi:10.1063/1.3656958.

29. Strickland, D.; Mourou, G. Compression of amplified chirped optical pulses. *Opt. Comm.* **1985**, *56*, 219–221.

30. Mourou, G.; Brocklesby, B.; Tajima, T.; Limpert, J. The future is fiber accelerators. *Nat. Photonics* **2013**, *7*, 258–261.

31. Nakajima, K. Conceptual designs of a laser plasma accelerator-based EUV-FEL and an all-optical Gamma-beam source. *High Power Laser Sci. Eng.* **2014**, *2*, doi:10.1017/hpl.2014.37.

32. Kostyukov, I.; Pukhov, A.; Kiselev, S. Phenomenological theory of laser-plasma interaction in "bubble" regime. *Phys. Plasmas* **2004**, *11*, 5256–5264.

33. Kalmykov, S.; Yi, A.; Khudik, V.; Shvets, G. Electron self-injection and trapping into an evolving plasma bubble. *Phys. Rev. Lett.* **2009**, *103*, doi:10.1103/PhysRevLett.103.135004.

34. Nieter, C.; Cary, J.R. VORPAL: An versatile plasma simulation code. *J. Comput. Phys.* **2004**, *196*, 448–473.

35. Lim, J.K.; Frigola, P.; Travish, G.; Rosenzweig, J.B.; Anderson, S.G.; Brown, W.J.; Jacob, J.S.; Robbins, C.L.; Tremaine, A.M. Adjustable, short focal length permanent-magnet quadrupole based electron beam final focus system. *Phys. Rev. ST Accel. Beams* **2005**, *8*, doi:10.1103/PhysRevSTAB.8.072401.

36. Association for Nuclear Technology in Medicine, Particle beam therapy facilities in Japan. Available online: http://www.antm.or.jp/05_treatment/04.html (accessed on 28 November 2014) (In Japanese).

37. Yasui, K. Current status and problems of particle beam therapy in advanced medical services for cancer. Available online: http://dl.ndl.go.jp/view/download/digidepo_8392376_po_075504.pdf (accessed on 28 November 2014) (In Japanese).